Hydrostatic pressure effects on superconducting transition of nanostructured niobium highly strained by high-pressure torsion

Journal of Applied Physics

Hydrostatic pressure effects on superconducting transition of nanostructured niobium highly strained by high-pressure torsion

Cite as: J. Appl. Phys. **125**, 125901 (2019); https://doi.org/10.1063/1.5083094
Submitted: 28 November 2018 . Accepted: 03 March 2019 . Published Online: 22 March 2019

Masaki Mito, Yuichiro Kitamura, Takayuki Tajiri, Kazuma Nakamura, Ryo Shiraishi, Kazuma Ogata, Hiroyuki Deguchi, Tomiko Yamaguchi, Nao Takeshita, Terukazu Nishizaki, Kaveh Edalati, and Zenji Horita

Journal of Applied Physics ARTICLE scitation.org/journal/jap

Hydrostatic pressure effects on superconducting transition of nanostructured niobium highly strained by high-pressure torsion

Cite as: J. Appl. Phys. **125**, 125901 (2019); doi: 10.1063/1.5083094
Submitted: 28 November 2018 · Accepted: 3 March 2019 ·
Published Online: 22 March 2019

Masaki Mito,[1,a)] Yuichiro Kitamura,[1] Takayuki Tajiri,[2] Kazuma Nakamura,[1] Ryo Shiraishi,[1] Kazuma Ogata,[1] Hiroyuki Deguchi,[1] Tomiko Yamaguchi,[1] Nao Takeshita,[3] Terukazu Nishizaki,[4] Kaveh Edalati,[5,6] and Zenji Horita[5,6]

AFFILIATIONS

[1]Graduate School of Engineering, Kyushu Institute of Technology, Kitakyushu 804-8550, Japan
[2]Faculty of Science, Fukuoka University, Fukuoka 814-0180, Japan
[3]National Institute of Advanced Industrial Science and Technology, Tsukuba 305-8568, Japan
[4]Department of Electrical Engineering, Kyushu Sangyo University, Fukuoka 813-8503, Japan
[5]Department of Materials Science and Engineering, Faculty of Engineering, Kyushu University, Fukuoka 819-0395, Japan
[6]International Institute for Carbon-Neutral Energy Research (WPI-I2CNER), Kyushu University, Fukuoka 819-0395, Japan

[a)]**Electronic address:** mitoh@mns.kyutech.ac.jp

ABSTRACT

We study the effects of hydrostatic pressure (HP) compression on the superconducting transition of severely strained Nb samples, whose grain sizes are reduced to the submicrometer level. Engineered granularity by high-pressure torsion (HPT) treatment changes the strength of coupling between submicrometer-scale grains and introduces lattice strain. We attempt to utilize the initially accumulated shear strain in the starting material for increasing the superconducting transition temperature T_c under HP compression. The HP effects on non-strained Nb have already been investigated in the pressure regime over 100 GPa by Struzhkin *et al.* [Phys. Rev. Lett. **79**, 4262 (1997)], and T_c reportedly exhibited an increase from 9.2 to 9.9 K at approximately 10 GPa. (1) Slightly strained Nb in the HPT treatment exhibits the increase in T_c under HP due to the strengthening of the intergrain coupling, so the pressure scale of the pressure response observed by Struzhkin *et al.* is reduced to approximately one-seventh at the maximum. (2) Prominently strained Nb in the HPT treatment exhibits the increase in T_c under HP due to a reduction in structural symmetry at the unit-cell level: In a Nb sample subjected to HPT (6 GPa, 10 revolutions), T_c exceeds 9.9 K at approximately 2 GPa. According to our first-principle calculations, the reduction in the structural symmetry affords an increase in the density of states at the Fermi energy, thereby yielding a prominent increase in T_c at low pressures.

I. INTRODUCTION

Bulk superconductivity characterized by macroscopic phase coherence exists in the Josephson array composed of superconducting grains. Generally, the carrier tuning at the unit-cell level is a method of intragrain manipulation to change superconducting transition temperatures (T_c). The change in the intergrain contact also influences T_c, and its control has sufficient possibility of increasing T_c.[1]

Hydrostatic pressure (HP) compression is useful for changing intergrain coupling[2,3] as well as carrier tuning at the unit-cell level.[4] The former effect prominently appears in weakly coupled granular networks. The pressure-induced structural transition observed in group 4 elements such as Ti, Zr, and Hf also promotes the increase in T_c.[5] Generally, as regards genuine pressure experiments of various superconductors, both pure samples and soft pressure-transmitting media (PTM) have been long desired. In such experiments, both initial shear strain in the sample preparation and additional shear strain by pressurization are intrinsically considered undesirable.

The superconductivity property depends on the sample quality that should be comprehensively evaluated from the viewpoints of both purity and residual strain. The shear strain reduces crystallinity,

and it is usually not favorable for realizing macroscopic coherence. However, it had already been known that it rarely works toward a favorable manner in thin film and amorphus Al,[6] Re,[7] and so on. Recently, it has been apparent that an enormous residual strain tuned intentionally can play a positive role in stabilizing superconductivity.[8,9]

In the field of material science, in order to create high-strength materials, researchers have utilized severe plastic deformation (SPD)[10,11] such as high-pressure torsion (HPT) [Fig. 1(a)],[12–15] equal-channel angular pressing,[16] and accumulative roll bonding.[17,18] The SPD process plays the role of accumulating dislocations, and the consequent grain refinement at the submicrometer or nanometer ranges is known to be effective in increasing the T_c of superconductors such as Nb[8] and Re[9] as well as creating good functionalities (e.g., high-strength materials).[19] The strain installed in the SPD process is relatively evaluated via a semi-experimental method. In the case of HPT, we can pursue the grain refinement as a function of revolution number N.

Here, we hypothesize that further stress application to strained materials subjected to the SPD process, considered as the so-called Josephson array of small grains similar to nanostructured Nb,[20] may lead to a new approach to increase T_c. Our strategy is to tune T_c by using two parameters such as N related to the initially installed strain [Fig. 1(a)] and pressure (P) related to the additional strain [Fig. 1(b)]. The latter can change the intergrain coupling through compression and tune the carrier density by deforming the lattice.

In this study, we target a conventional superconductor Nb, that is, a 4d transition metal with a bcc structure. It has the highest T_c at ambient pressure among simple elemental superconductors.[4] We conduct HP experiments on Nb samples subjected to SPD in the stage of sample preparation in the expectation of observing a high T_c as shown in Fig. 1 so that via the detailed study on the electro-structural correlation, we find a scientific route for increasing T_c in Nb. The results are compared with those for ceramic superconductors as a weakly coupled random Josephson network system.[2,3]

Below, we review the literature regarding superconducting transitions under the application of pressure. Table I lists previous studies that have examined HP effects on Nb. We note from the table that there is a wide variation in T_c with applied pressure across these studies.[21–27] We also note that most of the previous studies listed were conducted before 1970. Referring to the early studies in 1968–1969, we note that T_c increases at low pressure values:[23,24] for example, as per Gey's study in 1969, a Nb sample purified near the melting point exhibited an increase in T_c of 0.23 K at around 2.5 GPa, above which its value remained unchanged.[24] However, in the experiment using a 1:1 mixture of n-pentane and isoamyl alcohol (nP-iA) in 1970, T_c exhibited a decrease with a relative increase in pressure.[26] The most confident study based on NaCl as the PTM reported a slight decrease in T_c below 4 GPa, and T_c subsequently increased beyond this pressure.[27] At around 10 GPa, T_c exhibited a maximum value of approximately 9.9 K, beyond which T_c remained at approximately 9.8 K.[27] Thus, we note that the influence of residual strain and HP quality on the change in the $T_c(P)$ of Nb has already been recorded experimentally.[23,24,26,27] Against this backdrop, in the current study, we examine how the T_c of extremely strained Nb changes under conditions of nearly elastic stress, as illustrated in Fig. 1. Consequently, this tells us how lattice deformation is suitable to increase the T_c of Nb.

II. EXPERIMENTAL

Nb disks with a purity of 99.9% were cut with a diameter of 10 mm by a wirecutting electric discharge machine (EDM). As

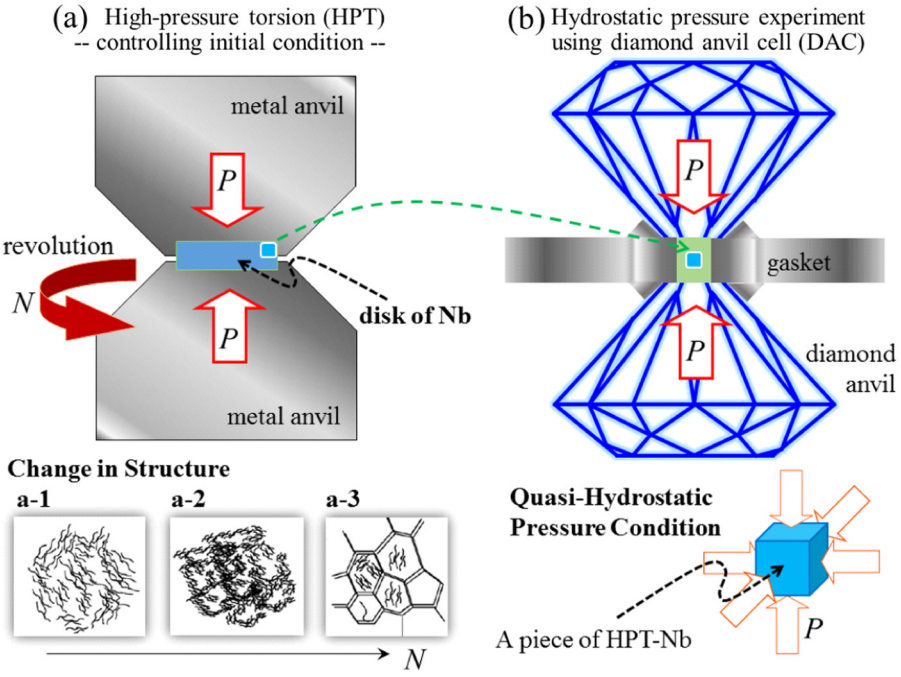

FIG. 1. Strategy of the present study. (a) In high-pressure torsion (HPT) for controlling the initial condition, by using two metal anvils, pressurization and revolution are conducted. As the revolution number (N) increases, dislocations are accumulated (a-1), and the grain size largely changes. The small-angle grain boundaries gradually transform to large-angle grain boundaries with an increase in N [(a-2) → (a-3)]. Finally, due to the balance between generation and annihilation of dislocations, the grain size remains unchanged despite the increase in N. (b) A few pieces of samples cut from the HPT-processed Nb are placed in a diamond anvil cell (DAC) to conduct the hydrostatic pressure (HP) experiment. Thereafter, the specimen is pressed in a quasi-HP condition using the DAC.

TABLE I. Previous studies on hydrostatic pressure (HP) experiments related to Nb. PTM: pressure-transmitting medium, nP-iA: 1:1 mixture of *n*-pentane and isoamyl alcohol, Ap-J: Apiezon-J oil, MEW: methanol–ethanol–water mixture in a volume ratio of 16:3:1, and O_2: condensed oxygen molecule. CY: cylindrical sample, AR: as-received sample, S: single-crystal, PO: polycrystal, SP: small pieces, PU: purified near the melting point, ARC: arc-melted, and HPT: high-pressure torsion. *N* denotes the revolution number of the HPT procedure performed at 6 GPa.

Year	Authors	Sample	Max. P (GPa)	$T_c(P=0)$ (K)	Initial dT_c/dP (K/GPa)	ΔT_c (K)	Max. T_c (K)	PTM	Ref.
1966	Gardner and Smith	CY/AR	ca. 1	9.4, 9.5	ca. 0	…	…	…	21
1966	Gey and Heyden	…	2.5	9.4, 9.5	ca. −0.03	…	…	…	22
1968	Köhnlein	…	4.1	9.40	+0.012	0.31	9.71 (4 GPa)	…	23
1969	Gey	PU	7.3	…	+0.11	0.23	…	…	24
1970	Brandt and Papp	CY	1.6	9.1	…	<0.1	…	Kerosene-oil	25
1970	Smith	S, PO	2.4	9.15–9.21	−0.016 to −0.025	−0.05	…	nP-iA	26
1997	Struzhkin *et al.*	SP	70	ca. 9.2	−0.025	0.7	9.9 (10 GPa)	NaCl	27
1997	Struzhkin *et al.*	SP	132	ca. 9.2	…	0.7	9.8 (15 GPa)	None	27
2019	Present work	AR	15.0	9.35	+0.09	0.38	9.78 (15.0 GPa)	Ap-J	…
2019	Present work	ARC	6	9.05	+0.14	0.26	9.31 (ca. 2 GPa)	Ap-J, MEW	…
2019	Present work	HPT ($N=1$)	6.0	9.35	+0.61	0.49	9.84 (ca. 1 GPa)	Ap-J	…
2019	Present work	HPT ($N=2$)	14.6	ca. 9.35	+0.33	0.38	9.79 (14.6 GPa)	Ap-J	…
2019	Present work	HPT ($N=5$)	10.1	ca. 9.35	+0.18	0.36	9.72 (ca. 2 GPa)	Ap-J	…
2019	Present work	HPT ($N=10$)	14.6	ca. 9.35	+0.29	0.57	9.92 (2.2 GPa)	Ap-J	…
2019	Present work	HPT ($N=10$)	6.2	ca. 9.35	+0.19	0.43	≥9.78 (6.2 GPa)	MEW	…
2019	Present work	HPT ($N=10$)	4.3	ca. 9.35	+0.03	0.08	9.43 (3.5 GPa)	O_2	…
2019	Present work	HPT ($N=10$)(cryo)	5.0	9.54	+0.18	0.38	9.92 (2.8 GPa)	Ap-J	…
2019	Present work	HPT ($N=20$)	5.6	ca. 9.35	+0.24	0.50	9.85 (2.4 GPa)	Ap-J	…

illustrated in Fig. 1(a), each of the disks was subjected to HPT processing at room temperature under a selected pressure of $P = 6$ GPa and revolutions of $N = 0$, 1, 2, 5, 10, and 20 with a rotation speed of 1 rpm.[8] Specimens with dimensions of approximately $0.8 \times 0.8 \times 0.5\,mm^3$ were cut from an HPT-processed disk using the EDM at the position of 2.5 mm from the disk center. The resistivity ρ for a series of specimens has been already measured: The residual resistivity ratio RRR [$=\rho(300\,K)/\rho(10\,K)$] is approximately 102 for the as-received (AR) sample, and it decreases an increase in N as from ∼ 103 ($N = 0$) to ∼23 ($N = 10$ and 20).[8] The above RRR values are between that for high-purity Nb (> a few hundred level) and that for granular Nb films in the dirty limit (1.5–8).[28] For $N = 10$, the HPT process was also performed at the liquid-nitrogen temperature [the corresponding sample is named $N = 10$(cryo)]. Here, we remark that for $N < 2$, dislocations are stored as illustrated in Fig. 1(a-1), and the grain size largely changes.[29] The small-angle grain boundaries formed in these cases gradually transform to large-angle grain boundaries an increase in N [corresponding to the change form Fig. 1(a-2) to Fig. 1(a-3)]. On the other hand, for $N \geq 2$, the fraction of large-angle grain boundaries increases due to an annihilation of dislocations at grain boundaries, and the grain size remains unchanged because of the balance between the dislocation generation by straining and the dislocation annihilation at grain boundaries. We note here that the average grain sizes for AR, $N = 2$, $N = 5$, and $N = 10$(cryo) samples have been reported to be 140 μm, 250 nm, 240 nm, and ca. 40 nm, respectively.[29,30] Thus, the shear insertion leads to a significant reduction in the grain size. The superconducting coherence length $\xi(0)$ for the single-crystal has been reported as around 20 nm,[31] and the aforementioned grain sizes for $N = 2$, $N = 5$, and $N = 10$(cryo) are at a level comparable with $\xi(0)$.[8] The penetration depth for the single-crystal is approximately 40 nm,[31] and a large superconducting signal observed in the present study reflects the intergrain coupling via grain boundaries. Further, at ambient pressure, T_c for AR is approximately 9.25 K, and T_c exhibits a maximum of approximately 9.37 K at $N = 2$. In addition, T_c remains unchanged at 9.35 K for $N > 10$.[8] In our study, for reference purposes, we also prepared arc-melted samples (ARC) whose residual strain was released. For the following HP experiment, small pieces with side lengths less than 0.1 mm were prepared as illustrated in Fig. 1.

Next, the AC magnetization of the samples was measured using a superconducting quantum interference device (SQUID) magnetometer equipped with an AC option. The frequency and the amplitude of the AC field were 10 Hz and 3.9 Oe, respectively. At a small amplitude of the AC field, the magnitude of the in-phase (m') is almost consistent with the Meissner signal observed at a static magnetic field.[32] Sufficiently below T_c, there is no out-of-phase component reflecting energy loss, and m' is related with the volume fraction of magnetic shielding. However, the signal associated with the superconducting transition is proportional to $v/(1-D)$, where v and D are volume of the sample and demagnetization factor of the sample, respectively.[33,34] When the sample gets thinner and D approaches 1, an enhancement of the superconducting signal occurs. Herein, we pay much attention to the shift of the superconducting signal in m' along the temperature axis. The T_c values were estimated from the onset of the superconducting signal, similar to the manner adopted by Struzhkin *et al.*[27] In the small pressure region, the superconducting signal sometimes became broad. Thus,

the onset temperature was evaluated as the confident T_c after the quantitative deviation of the onset temperature was confirmed to be consistent with that of the midpoint temperature.

Contraction corresponding to a stress of up to 15 GPa was achieved using a miniature CuBe diamond anvil cell (DAC) that consisted of two diamond anvils with flat tips having a diameter of 0.5 mm and a 0.25-mm-thick Re gasket.[35] In the HP-type experiments, liquid-like PTMs such as Apiezon-J oil (Ap-J) and MEW (methanol–ethanol–water mixture in the volume ratio of 16:3:1) and condensed oxygen molecule (O_2) were confined together with small pieces of Nb in the sample chamber: At room temperature, Ap-J solidifies at a few kbar, and MEW remains in the liquid state until 10 GPa.[36] O_2 solidifies at approximately 6 GPa at room temperature, whereas solid O_2 realizes better HP quality at liquid helium temperature than solidified MEW. The pressure value at room temperature (P_{rt}) was evaluated by measuring the fluorescence of ruby[37] located in the sample chamber with the Nb pieces. According to Ref. 35, when temperature is cooled from room temperature to liquid helium temperature, there appears the pressure increase equal to approximately 10% of P_{rt}. In this paper, P_{rt} is adopted as the pressure value (P) in each measurement, since the comparison between the magnetic and structural data at low pressures of $P < 5$ GPa is meaningful.

Furthermore, to determine the structural shrinkage under pressure, we performed X-ray diffraction (XRD) analyses under a high pressure of up to $P = 5.1$ GPa at room temperature using a synchrotron radiation XRD system with a cylindrical imaging plate at the Photon Factory at the Institute of Materials Structure Science, High Energy Accelerator Research Organization.[38] The energy of the incident X-rays was 16 keV. Pressure was applied using a DAC that consisted of two diamond anvils with flat tips having a diameter of 0.8 mm and a 0.3-mm-thick CuBe gasket. The small pieces of HPT-Nb were placed in a randomly oriented manner in a sample cavity with a diameter of 0.4 mm along with a ruby of manometer and transparent PTMs such as fluorinated oil (FC77, Sumitomo 3M Ltd.) or MEW. Transparent FC77 undergoes solidification below 1 GPa at room temperature[39] similar to brown Ap-J with the ease of handling for the miniature DAC, contrary to liquid MEW below 10 GPa.[36] All the atomic positions in the body-centered cubic (bcc) structure are special positions, and therefore, the structural parameters can be evaluated just with the use of the diffraction peak angle. The lattice parameters were estimated using all of the observed diffraction peaks: In the experiments of using DAC, we used five diffraction peaks of the plane indices (110), (200), (211), (220), and (310). In the measurements with glass capillary, the three peaks (222), (321), and (400) were also considered in addition to the above five peaks.

III. CRYSTAL STRUCTURE AT AMBIENT PRESSURE

Prior to the experiments on hydrostatic pressure, we mention the crystal structure in the unit cell level for the targeted samples. Figure 2(a) shows the XRD profiles corresponding to the (110) plane diffraction of the bcc structure. The magnitude of the residual shear strain increases in the turn of ARC → AR → $N = 1$ → 2 → 5 → 10 → 20. The position of the diffraction peak of the (110) plane for AR is shown with the dotted line. It slightly shifts toward high angle sides in the turn as ARC → AR → $N = 1$ → 2 → 5. However, between $N = 5$ and 10, there occurs the sudden shift toward the low angle side. In the process of $N = 10$ → 20, it moves to the high angle side again. When this structure change is analyzed in the framework of the bcc structure, we find a remarkable jump in the lattice parameter between $N = 5$ and 10 in the trend of its decrease with an increase in N as shown in Fig. 2(b). There is no distinct change such as splitting of diffraction peaks, whereas it might be natural to assume any structural distortion such as the change from cubic to strained bcc [for instance, body-centered orthorhombic (bco) or tetragonal (bct)]. Rietveld analysis for AR

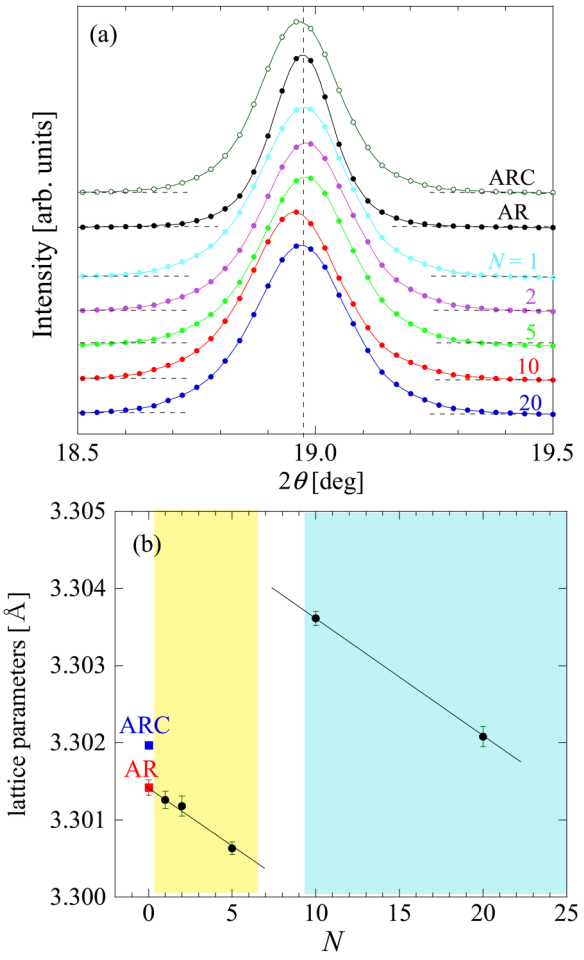

FIG. 2. (a) XRD profiles of arc-melted Nb (ARC-Nb), as-received Nb (AR-Nb), and HPT-Nb ($N = 1$, 2, 5, 10, and 20) samples. The wavelength of the incident X-ray was 0.77160 Å. The peaks correspond to the (110) plane diffraction of the bcc structure. (b) Lattice parameters estimated via analysis of the XRD profiles. Herein, for all of ARC-Nb (blue closed square), AR-Nb (red closed square), and HPT-Nb (black closed circle), the bcc system is assumed. The data for both ARC-Nb and AR-Nb are plotted at the zero coordinate of the horizontal axis. The solid and dotted lines serve as visual guides. The yellow and light blue colors represent that there seems to be a discontinuous change between $N = 5$ and 10.

presents the fitting based on bcc ($Im\bar{3}m$) ($R_{wp} = 10.1$) is better than that on bco ($Immm$) ($R_{wp} = 11.6$). However, for $N = 10$, bco ($R_{wp} = 6.3$) is better that bcc ($R_{wp} = 8.8$). Anyway, as a first approach, the analysis based on the bcc structure is convincing.

IV. EXPERIMENTAL RESULTS UNDER HYDROSTATIC PRESSURE

A. AC magnetization

AR-Nb. Figures 3(a) and 3(b) show the experimental results of the AC magnetization of the AR-Nb sample. AR samples are subjected to pressing and rolling, and they initially carry some residual strain at the grain and unit-cell levels. Over two experimental runs, we confirmed that AR exhibits an almost monotonic shift of the superconducting signal towards the high-temperature regime with an increase in pressure. Figure 3(e) illustrates the pressure dependence of its T_c along with those for ARC-Nb. The T_c values were estimated from the onset of the superconducting signal, plotted with those evaluated from the midpoint. We note that T_c increases linearly against pressure within the initial pressure regime below 2 GPa, and its behavior is similar to that reported by Köhnlein.[23] However, at around the characteristic pressure P_c of 2 GPa, there is a minute cusp, and finally, the T_c value gradually increases to 9.78 K at $P = 15.0$ GPa.

ARC-Nb. Figures 3(c) and 3(d) show the temperature dependence of the AC magnetization of ARC-Nb. ARC-Nb exhibits a maximum T_c at around $P = 2 - 3$ GPa, which is close to the

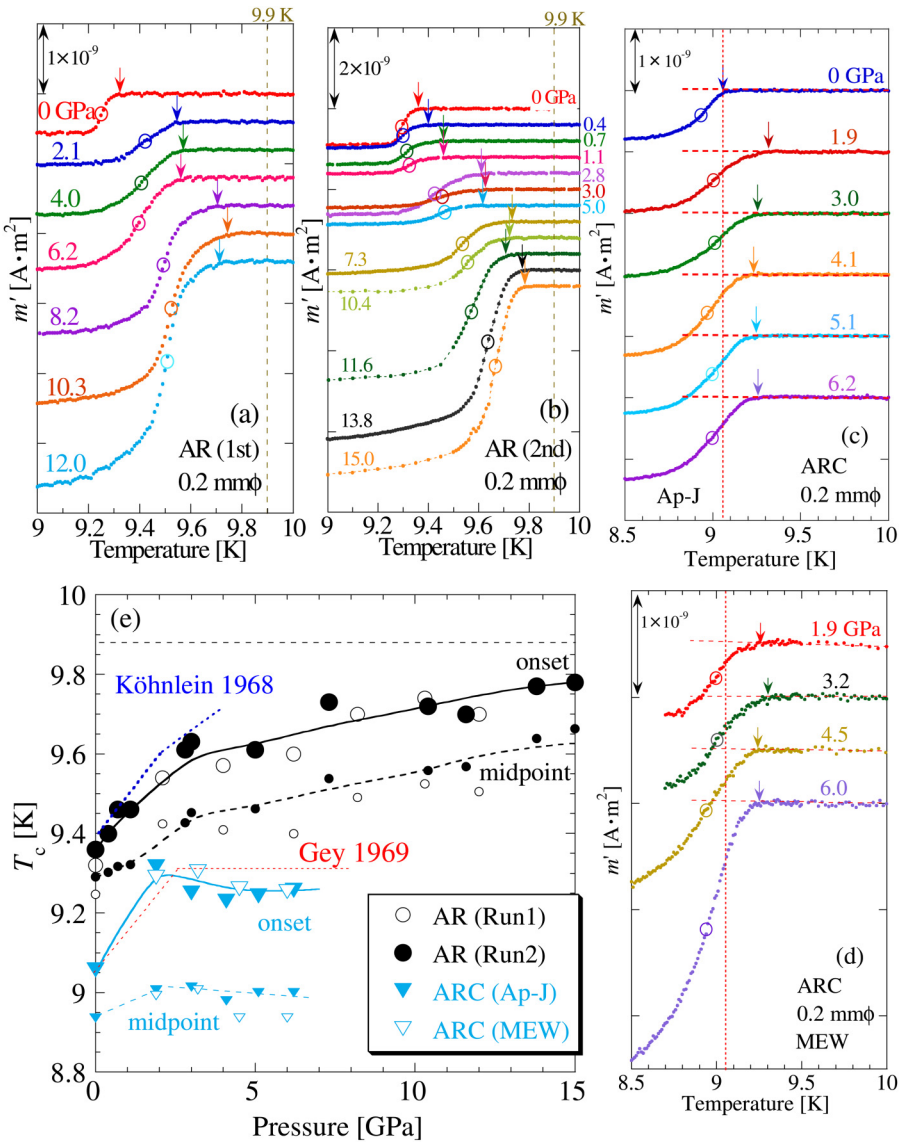

FIG. 3. Temperature dependence of AC magnetization for as-received (AR) (a) and (b) and arc-melted (ARC) samples (c) and (d) at various pressures. In all measurements, the diameter of the sample chamber was 0.2 mm. The onset of the superconducting signal is presented with an arrow, and the midpoint is marked with an open circle. For the AR samples, Ap-J was used as the PTM. In the case of the ARC samples, two kinds of PTMs, Ap-J (c) and MEW (d), were used. (e) Pressure dependence of superconducting transition temperature T_c for both AR-Nb and ARC-Nb samples. The T_c values estimated from the onset of the superconducting signal were connected with the change in the midpoint temperature (the corresponding small symbol). The initial behavior of T_c of the AR sample is similar to that observed by Köhnlein in 1968.[23] The overall behavior of T_c of the ARC sample is similar to that observed in the sample purified near the melting point by Gey in 1969.[24]

aforementioned P_c value for AR-Nb. Subsequently, T_c exhibits a minimum at around $P = 5$ GPa, exhibiting a plateau at 9.25 K. This behavior is more similar to that reported by Gey for a sample purified near the melting point[24] than Köhnlein's result,[23] so that we recognize the effect of melting for releasing strain. This behavior was observed independently of PTMs such as Ap-J and MEW. Thus, in ARC-Nb, there is no significant difference in the observed results with the change of the PTM. A T_c difference of 0.2 K continually exists between $T_c(P)$ of AR and that of ARC.

HPT-Nb for $N = 1$, 2, and 5. We next present the results for HPT-Nb samples. A small degree of HPT processing inserts a dislocation into the AR sample, thereby resulting in a prominent weakening of intergrain coupling as well as a decrease in the grain size.[29] Figure 4 shows the temperature dependence of the AC magnetization of HPT-Nb for $N = 1$–5. In general, the results for $N = 1$, 2, and 5 are qualitatively similar to those of the AR samples. The T_c values for $N = 1$, 2, and 5 at $P > 10$ GPa approach that of the AR sample. In each case, the cusp appears in the pressure regime below 5 GPa. We first note that the P_c value for $N = 1$ is 1.5 ± 0.7 GPa, which is smaller than those of both AR and ARC. Next, we note that P_c increases with an increase in N from $1 \rightarrow 2 \rightarrow 5$, whereas the maximum T_c at P_c systematically decreases with an increase in N.

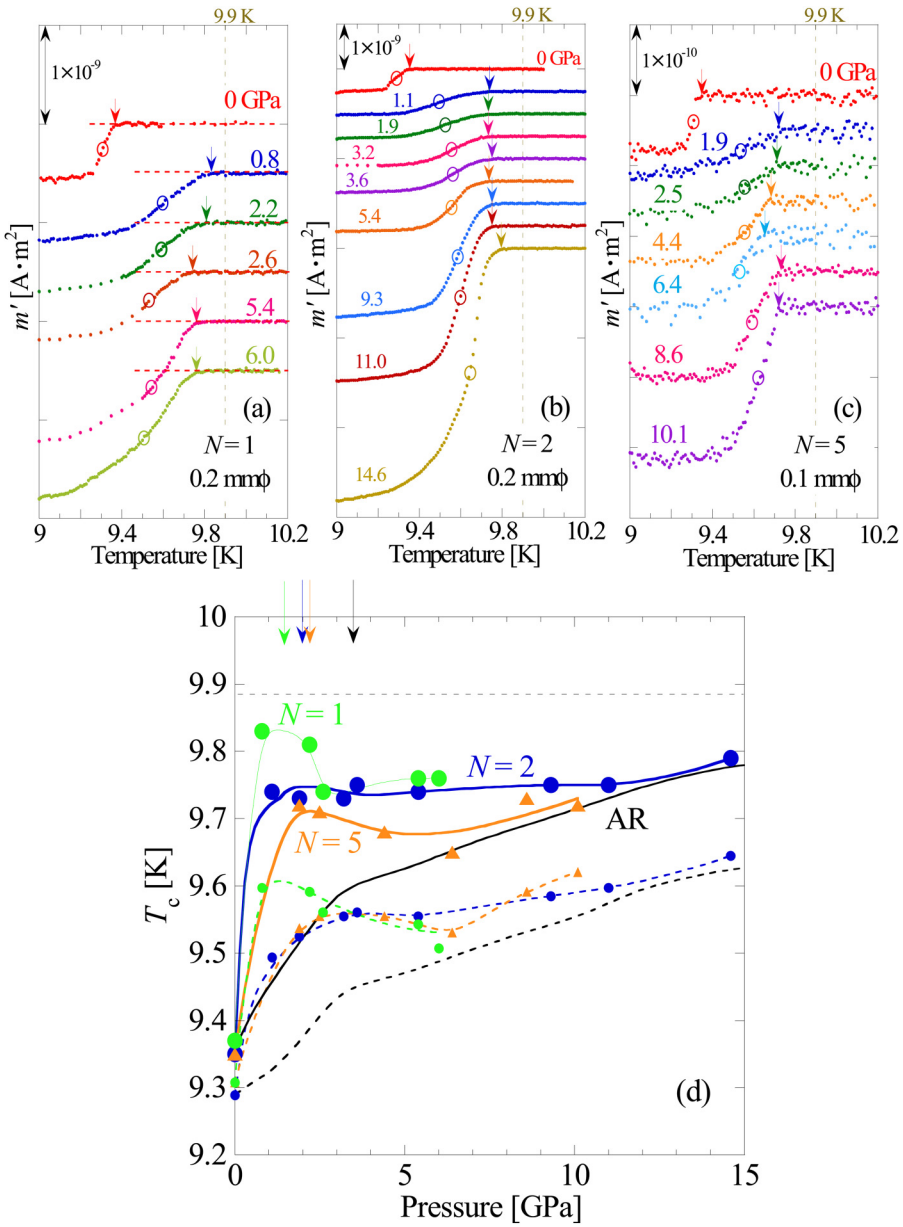

FIG. 4. Temperature dependence of AC magnetization for HPT-Nb samples with $N = 1$ (a), 2 (b), and 5 (c) at various pressures. The diameter of the sample chamber for $N = 1$ and 2 was 0.2 mm, and that for $N = 5$ was 0.1 mm. The onset of the superconducting signal is presented with an arrow, and the midpoint is marked with an open circle. (d) Pressure dependence of superconducting transition temperature T_c for HPT-Nb for $N = 1$, 2, and 5. The T_c values estimated from the onset of the superconducting signal (the large symbol with a solid curve) were connected with the change in the midpoint temperature (the corresponding small symbol with a broken curve). Arrows represent the values of characteristic pressure P_c. For three samples, Ap-J was used as the PTM. For reference, the guide curves corresponding to $T_c(P)$ of the AR sample with Ap-J as the PTM [see Fig. 3(e)] are also presented with the black solid (onset) and broken (midpoint) curves.

The insertion of the dislocation and the reduction in grain size, which occur during the process from AR to HPT application with $N = 1$, enhance the T_c value at P_c. However, further strain insertion suppresses the increase in the T_c value.

HPT-Nb for $N = 10$. Figures 5 and 6 show the temperature dependence of the AC magnetization of HPT-Nb for $N = 10$. For $N = 10$ using Ap-J as PTM, a drastic increase in T_c is observed at around 2 GPa. The change is not on the elongated line of the change from $N = 1$ to 5. Indeed, as seen in Figs. 5(a) and 5(b), T_c for $N = 10$ at P_c is greater than 9.9 K, and even for $P > P_c$, the T_c value remains high at approximately 9.8 K [see Fig. 5(d)]. Thus, between $N = 5$ and 10, there is a drastic jump in $T_c(P)$. Here, we stress that the pressure dependence of T_c for $N = 10$ depends on the type of PTM used, contrary to the results for the ARC samples [as shown in Figs. 3(c)–3(e)]. In this context, we note that the PTM MEW[36] and O_2[40] do not undergo solidification at room temperature when $P < 5$ GPa. When HPT-Nb ($N = 10$) is pressurized in liquid-medium MEW at room temperature, T_c once exhibits a plateau below 3 GPa after its initial increase, as seen in Figs. 6(a) and 6(c). Above approximately 3 GPa, it prominently increases, and at around 6-7 GPa, it approaches the value using Ap-J as PTM. With the use of O_2 as a higher-quality PTM at low temperatures, T_c does not exhibit a meaningful increase at pressures of up to 4.3 GPa [see Figs. 6(b) and 6(c)]. The overall sample behavior across the experiments with AP-J, MEW, and O_2 suggests that the pressure dependence of T_c depends on the quality of HP (based on the PTM used). Consequently, it appears that the pressure conditions at room temperature affect the change in the crystal structure.

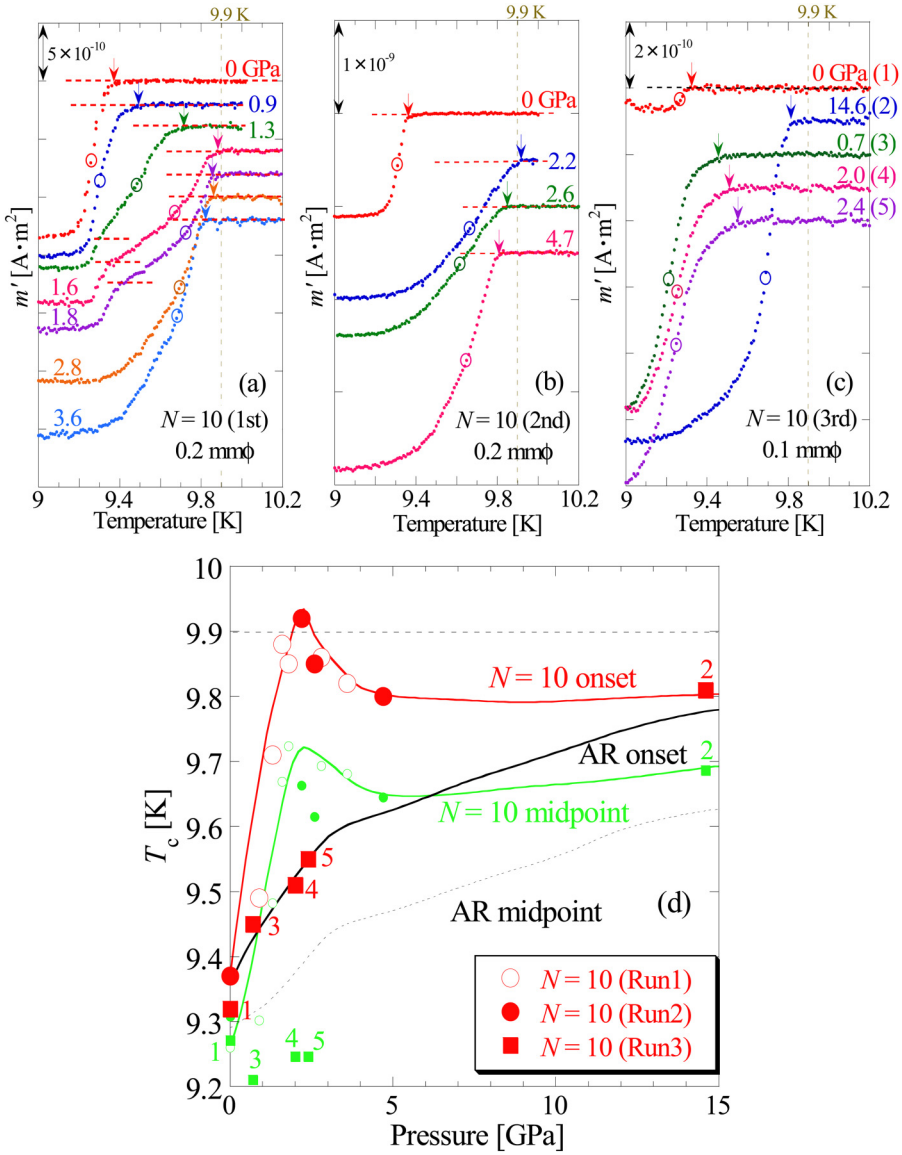

FIG. 5. Temperature dependence of AC magnetization for HPT-Nb samples with $N = 10$ using Ap-J as PTM [first run (a), the second (b), and the third (c)] at various pressures. The diameter of the sample chamber for the first and second runs was 0.2 mm and that for the third run was 0.1 mm. The onset of the superconducting signal is presented with an arrow, and the midpoint is marked with an open circle. For $P = 1.3$, 1.6, and 1.8 GPa in (a), the midpoint was evaluated for the major superconducting signal. The number beside the pressure value in (c) indicates the measurement trial number. (d) Pressure dependence of superconducting transition temperature T_c for HPT-Nb with $N = 10$. The T_c values estimated from the onset of the superconducting signal (the large symbol with a solid curve) were connected with the change in the midpoint temperature (the corresponding small symbol with a solid curve). Here, Ap-J was used as the PTM. The number beside each symbol indicates the measurement trial number in the third run. For reference, the guide curves corresponding to $T_c(P)$ of the sample AR using Ap-J as PTM [see Fig. 3(e)] are also presented with the black solid (onset) and broken (midpoint) curves.

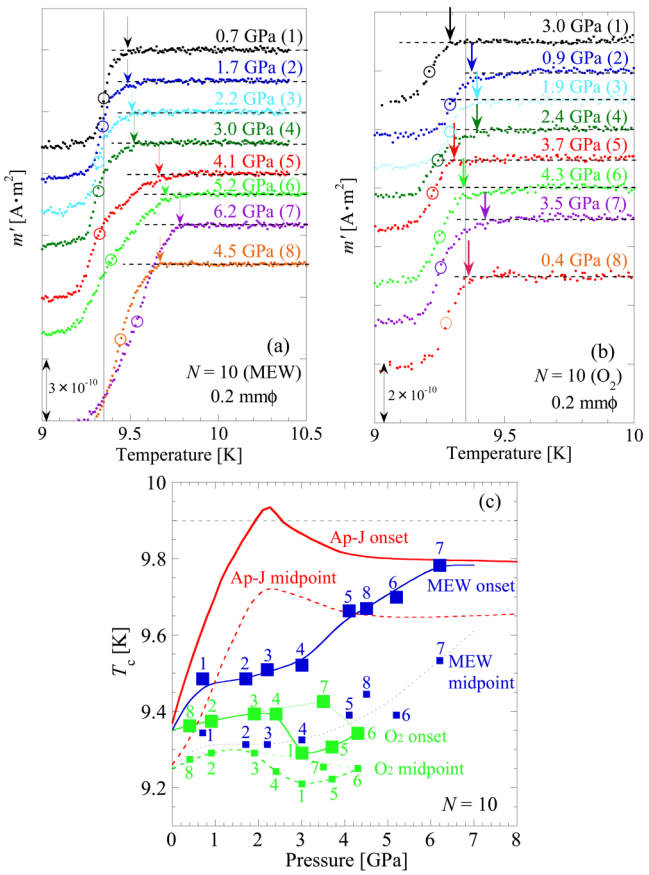

FIG. 6. Temperature dependence of AC magnetization for HPT-Nb samples with $N = 10$ using MEW (a) and O_2 (b) as PTM. In both measurements, the diameter of the sample chamber was 0.2 mm. The onset of the superconducting signal is presented with an arrow, and the midpoint is marked with an open circle. (c) Pressure dependence of superconducting transition temperature T_c for HPT-Nb with $N = 10$ using MEW and O_2 as PTM. The T_c values estimated from the onset of the superconducting signal (the large symbol with a solid curve) were connected with the change in the midpoint temperature (the corresponding small symbol). The numbering alongside each of the symbols indicates the measurement trial number. For reference, the guide curves corresponding to $T_c(P)$ of the HPT-Nb samples with $N = 10$ using Ap-J as PTM [see Fig. 5(d)] are also presented with the red solid (onset) and broken (midpoint) curves.

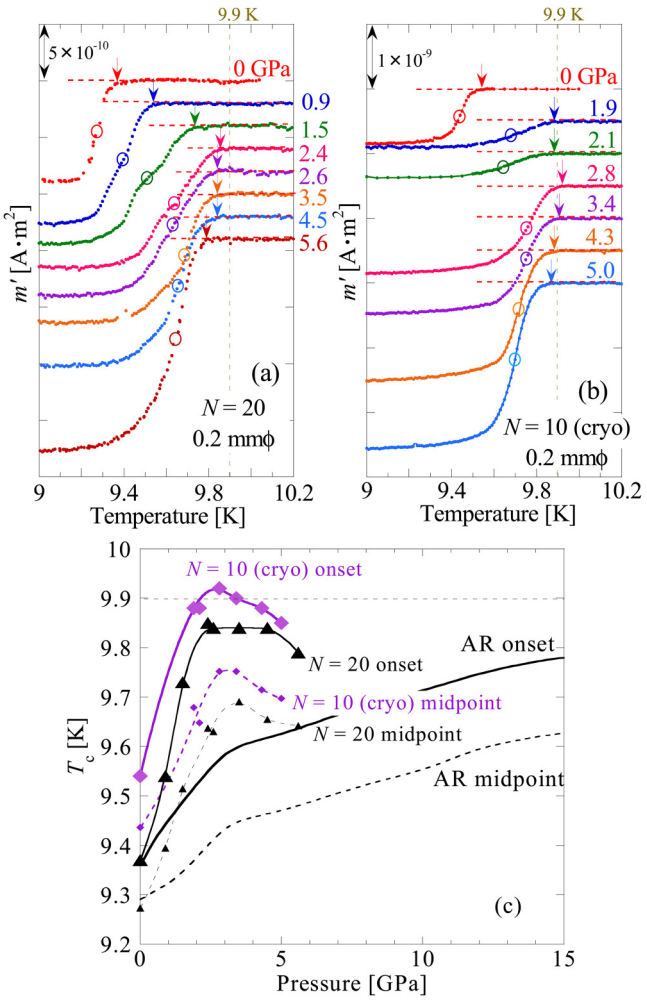

FIG. 7. Temperature dependence of AC magnetization for HPT-Nb samples with $N = 20$ (a) and 10(cryo) [subjected to the HPT procedure near the liquid-nitrogen temperature] (b) at various pressures. In both measurements, the diameter of the sample chamber was 0.2 mm. The onset of the superconducting signal is presented with an arrow, and the midpoint is marked with an open circle. (c) Pressure dependence of superconducting transition temperature T_c for HPT-Nb with $N = 20$ and 10(cryo). The T_c values estimated from the onset of the superconducting signal (the large symbol with a solid curve) were connected with the change in the midpoint temperature (the corresponding small symbol with broken curve). In both sets of measurements, Ap-J was used as the PTM. For reference, the guide curves corresponding to $T_c(P)$ of AR using Ap-J as PTM [see Fig. 3(e)] are also presented with the black solid (onset) and broken (midpoint) curves.

Thus, it is necessary to understand how the structure changes with the change in the PTM. We consider this topic again in the context of XRD measurements in subsection IV B.

HPT-Nb for $N = 10$(cryo) and 20. Figure 7 shows the temperature dependence of the AC magnetization of HPT-Nb for $N = 10$(cryo) and 20. Next, we reconsider the experiment using Ap-J as the PTM. As for $N = 10$(cryo) with a significantly smaller grain size, the maximum T_c is almost the same as that for $N = 10$, and P_c is slightly higher than that for $N = 10$ when using Ap-J. The reduction of the grain size to a few hundred nanometers reflects as the highest T_c at $P = 0$ among a series of samples. A comparison of the $N = 10$ and $N = 10$(cryo) data suggests that the main factor influencing T_c of above 9.9 K is *neither the grain size nor the intergrain network*; rather, we need to consider *the strain at the unit-cell level*. Finally, we note that the results for $N = 20$ resemble those for $N = 10$(cryo), and the maximum T_c is below 9.9 K. Across our series of experiments, the experiments for $N = 10$ and $N = 10$(cryo) yield the highest T_c, exceeding 9.9 K.

Pressure dependence of T_c using Ap-J. Herein, we remember the pressure dependence of T_c for all the aforementioned samples with the use of Ap-J as the PTM. The remarkable difference between the data for ARC and those for other HPT materials indicates that the magnitude of the residual strain at the starting point (i.e., at $P = 0$) in a series of pressure experiments influences the change in T_c under HP. Indeed, severely strained Nb exhibits the maximum T_c in the low-pressure range: For instance, the $N = 1$ and 10 samples exhibit the optimal T_c over 9.8 K at around 1 GPa [see Fig. 4(d)] and that over 9.9 K at around 2 GPa [see Fig. 5(d)], respectively. We also observe drastic jumps in the curves between AR and $N = 1$ (see Figs. 3 and 4), and between $N = 5$ and 10 (see Figs. 4 and 5). For $P > 10$ GPa, the $T_c(P)$ curves tend to coincide with the data for AR, and there is no significant behavioral difference between the samples except for ARC. In a previous study by Struzhkin *et al.*, Nb reportedly exhibited the highest T_c of 9.9 K at around 10 GPa.[27] Here, when we reduced the pressure scale down by a factor of one-fifth, we observed that the pressure dependence of T_c for $P < 80$ GPa as reported by Struzhkin *et al.*[27] was fairly consistent with the results of HPT-Nb ($N = 10$) with the use of Ap-J below 15 GPa [see Fig. 5(d)]. T_c for HPT-Nb ($N = 1$) becomes similar to the result of Struzhkin *et al.*[27] by scaling down with a factor of one-seventh. This result characterizes both the existence of the universal behavior of $T_c(P)$ and the effect of the initial shear strain on $T_c(P)$. In order to check how the crystal structure at the unit-cell level changes under pressure for each sample type, we next conducted XRD experiments on the representative samples under the application of pressure.

B. XRD

Prior to describing the structural changes under pressure, we briefly discuss the change in crystallite size. It has been experimentally determined that the crystallite size evaluated via analysis of the full-width at half-maximum (FWHM) values of the XRD profiles is smaller than the grain size obtained by surface observations. Further, our FWHM analysis indicates that the crystallite size hardly changes with pressurization. Thus, considering that there is no prominent change in the grain size, we focus on changes in the structural parameters of the unit cell.

Pressure dependence of normalized interplanar distances. Figure 8 depicts the pressure dependence of the normalized interplanar distances for ARC, AR, and HPT-Nb ($N = 1$, 5, and 10) samples in the case of considering the bcc lattice. The pressure regime corresponding to the anisotropic structure change is highlighted in light blue. Transparent fluorine oil FC77 was used as the PTM, and particularly for HPT-Nb ($N = 10$), MEW was also used. FC77 belongs to the same group with dense liquid PTM type of Ap-J in such sense that they solidify at pressure of below 1 GPa. As can be observed in Fig. 8(a), ARC exhibits isotropic shrinkage, wherein the slope of the curve (−0.15%/GPa) is slightly lesser than that obtained with the use of MEW (−0.18%/GPa), as reported by Takemura *et al.*[41] From Fig. 8(b), we observe that AR exhibits an isotropic lattice change of −0.26%/GPa for $P \leq 2$ GPa. The slope value is larger than the two aforementioned values. For $2 < P < 3$ GPa, all interplanes except for the (310) interplane expand and subsequently shrink again. When the AR sample is subjected to the HPT process with $N = 1$, the resultant interplanar behavior in

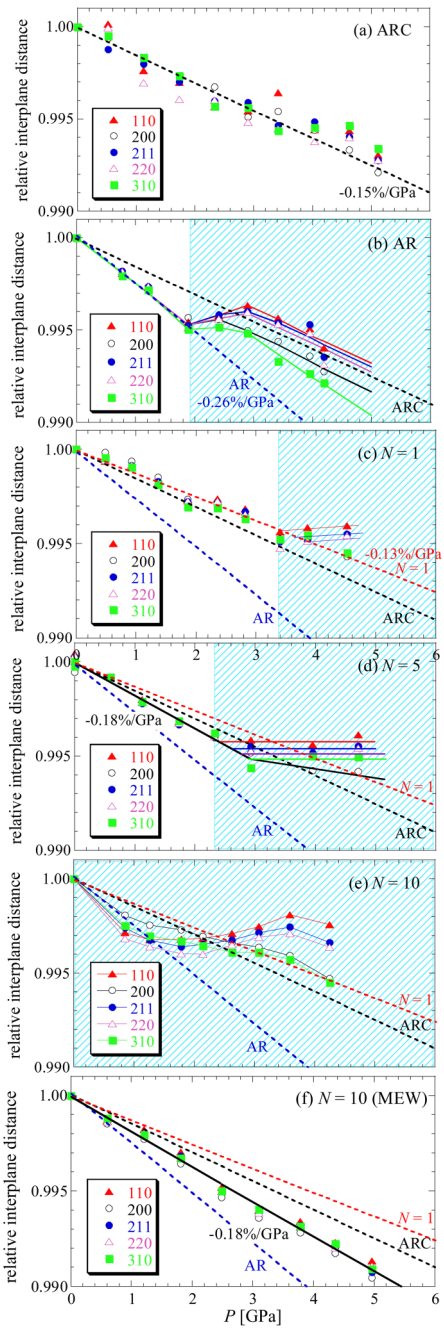

FIG. 8. Pressure dependence of normalized interplanar distance of (110), (200), (211), (220), and (310) planes for ARC (a), AR (b), and HPT-Nb samples for $N = 1$ (c), 5 (d), and 10 (e) and (f). The broken guide lines in all figures represent the interplanar distance change for ARC (black), AR (blue), and $N = 1$ (red). The initial slope value in the pressure regime where the isotropic structure change occurs is also indicated. The pressure regime corresponding to the anisotropic structure change is indicated in light-blue hatching. Except for the measurement (f) corresponding to the use of MEW as the PTM, FC77 was used as PTM in all other cases.

TABLE II. Initial slope corresponding to relative interplanar distance for ARC, AR, and HPT-Nb(N) samples in the pressure regime where isotropic structure change occurs. P'_c stands for the upper limit of the pressure regime where the isotropic structure change occurs (see Fig. 8). Notation pw indicates the present work.

Sample	ARC	AR	$N = 1$	$N = 5$	$N = 10$	$N = 10$	Unstrained	Unstrained
PTM	FC77	FC77	FC77	FC77	FC77	MEW	MEW	^{4}He
Ref.	pw	pw	pw	pw	pw	pw	41	41
Initial slope (%/GPa)	−0.150	−0.256	−0.126	−0.180	…	−0.184	−0.180	−0.190
P'_c (GPa)	> 5.2	1.9	3.4	2.3	0	> 5.0	10	…

Fig. 8(c) approaches that of the ARC sample [see Fig. 8(a)]. Isotropic shrinkage with the smallest slope (−0.13%/GPa) is observed among the target samples. This phenomenon suggests that the process of reducing the grain size effectively plays the role of releasing the residual strain of the AR sample at the unit-cell level. However, slight expansion of (110), (211), and (220) interplanes appears at around $P = 3.5$ GPa. Further increase in the revolution number of the HPT process up to $N = 5$ [Fig. 8(d)] and 10 [Fig. 8(e)] induces an anisotropic change in the interplanar distance at smaller pressure. For $N = 5$, an increase in the interplanar distance except for the (200) interplane is observed at around $P = 3$ GPa after isotropic shrinkage with a slope of −0.18%/GPa. For $N = 10$, anisotropic shrinkage occurs at quite small pressures: A temporary increase in the interplanar distance is observed over a wide pressure range of $1.5 < P < 3.5$ GPa, whose range is wider than those for AR and HPT-Nb ($N = 1$ and 5) samples. On the other hand, the $N = 10$ sample using MEW exhibits isotropic shrinkage with a slope of −0.18%/GPa, which is close to those for $N = 1$ and non-strained Nb using MEW, as reported by Takemura *et al.*[41] This result indicates that the anisotropic structure change is influenced by both the initial strain, controllable as a function of N, and the HP quality. Across the torsion process from $N = 1$ to 10, an enormous strain is expected to be induced in the unit-cell level. In this case, stress application with the use of a solidified PTM is effective. Given the aforementioned information, we summarize both the upper limit P'_c of the region of the isotropic structure change and the initial slope of the relative interplane distance in Table II.

Pressure dependence of lattice deformation. Given the results of Fig. 8, we perform the following analyses: (1) analyzing lattice constant based on cubic lattice (a_{cubic}), (2) analyzing lattice parameters along three principal directions (a_1, a_2, and a_3), and (3) evaluating anisotropic lattice deformation using a_1/a_{cubic}, a_2/a_{cubic}, and a_3/a_{cubic}. Figure 9 depicts the pressure dependence of a_1/a_{cubic}, a_2/a_{cubic}, and a_3/a_{cubic} for ARC, AR, and HPT-Nb ($N = 1$, 5, and 10) samples. Anisotropic deformation is prominent at the experiments for AR and HPT-Nb ($N = 10$) using FC77 as PTM. In the case of both the AR and the $N = 1$, 5, and 10 samples, there are observed small lattice distortions of less than 1% against a_{cubic} along each principal direction. At pressures below a critical pressure P'_c ($P < P'_c$), the unit cell shrinks isotropically along all of the three-dimensional principal directions. Thus, the cell shrinks under isotropical stress at $P < P'_c$, whereas at P'_c, it releases the accumulated heavy strain, thereby resulting in a significant expansion along any direction. For $P > P'_c$, indeed, there should be expansion along any direction as well as shrinkage along a direction. As for $N = 10$, anisotropic structure change is observed over a wide pressure regime.

Herein, we explain the detailed analytic results for HPT-Nb ($N = 10$) at $P = 4.3$ GPa shown in Fig. 9(e): We obtained $a_{cubic} = 3.2739$ Å, $a_1 = 3.2683$ Å, $a_2 = 3.2910$ Å, and $a_3 = 3.2974$ Å. Thus, the cubic lattice shrinks toward one direction characterized with a_1, and it expands toward the directions perpendicular to the shrinkage axis. The cubic lattice tends to be distorted toward tetragonal rather than orthorhombic. This anisotropic deformation does not occur when MEW is used as the PTM, thus suggesting that the non-hydrostatic pressurization at room temperature triggers this phenomenon. Here, we remark that the elucidation of the effect of anisotropic shrinkage on the superconducting transition may yield a solution to effectively increase T_c.

C. First-principles calculation

From the viewpoint of scientific interest in $T_c(P)$, the most evident increase in T_c was observed in HPT-Nb ($N = 10$). Thus, it is of interest to understand whether or not the anisotropic structure change from the bcc to the orthorhombic system close to the tetragonal lattice actually leads to the T_c increase.

Consequently, we performed density-functional calculations for Nb using the extended version of the Tokyo Ab-initio Program Package[42] with plane-wave basis sets, where norm-conserving pseudopotentials[43,44] and the generalized gradient approximation of the exchange-correlation potential[45] were employed. The cutoff energies in the wavefunction and charge densities were 64 and 256 Ry, respectively, and the $40 \times 40 \times 40$ k-point sampling was employed. The electronic density of states (DOS) was calculated by means of the generalized tetrahedron method.[46,47]

Based on experimental trends in the lattice change, we first focus on the specific deformation of the body-centered cubic (bcc) structure to the body-centered tetragonal (bct) structure, which is schematically shown in Fig. 10. The deformation is expressed as $(a, a, a) \rightarrow (a', a', c')$ with $a' = (1 + \delta)a$ and $c' = (1 - \delta)a$. In the present calculation, we assume $a = 3.29$ Å and $\delta = 0.015$. The Bravais lattice is expressed for a bcc system as

$$a_1 = \frac{a}{2}(-1, 1, 1),$$
$$a_2 = \frac{a}{2}(1, -1, 1),$$
$$a_3 = \frac{a}{2}(1, 1, -1)$$

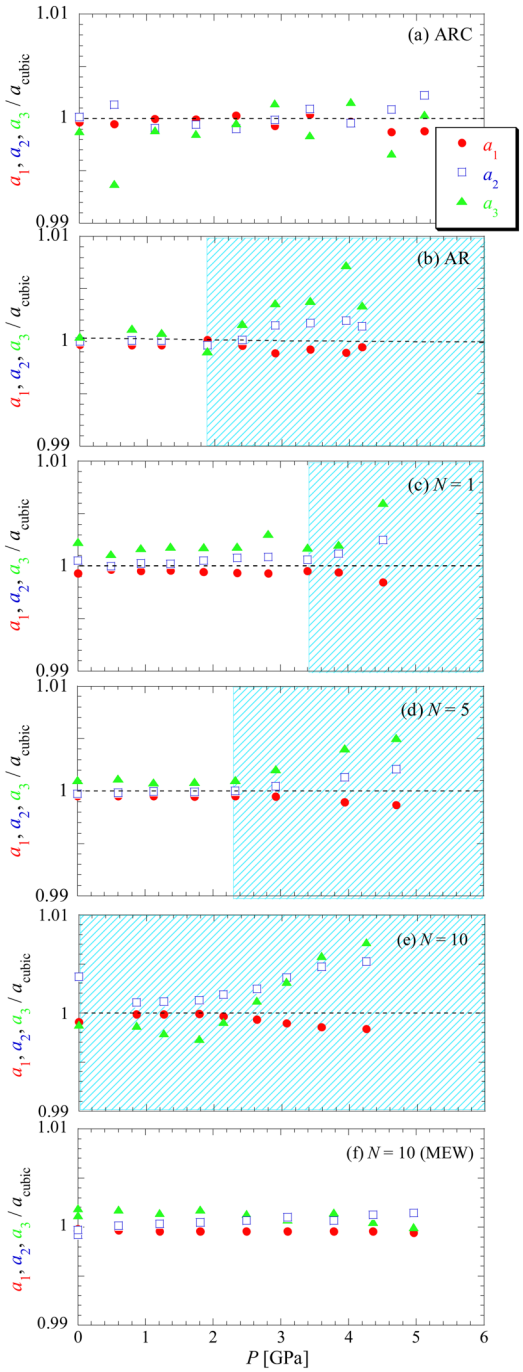

FIG. 9. Pressure dependence of anisotropic lattice deformation using normalized lattice constants a_1/a_{cubic}, a_2/a_{cubic}, and a_3/a_{cubic} for ARC (a), AR (b), HPT-Nb for $N = 1$ (c), $N = 5$ (d), and $N = 10$ (e) and (f) samples. a_{cubic} is a lattice constant considering the bcc lattice. The pressure regime corresponding to the anisotropic structure change, determined in Fig. 8, is indicated in light-blue hatching. Except for the measurement (f) with the use of MEW as the PTM, FC77 was used as the PTM in all other cases.

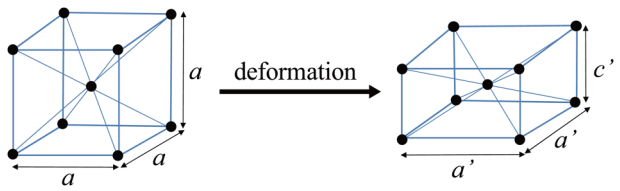

FIG. 10. Schematic of lattice deformation, where a bcc lattice (left panel) is deformed to a bct lattice (right panel).

and for a bct system as

$$a_1 = \frac{a}{2}[-(1+\delta), 1+\delta, 1-\delta],$$
$$a_2 = \frac{a}{2}[1+\delta, -(1+\delta), 1-\delta],$$
$$a_3 = \frac{a}{2}[1+\delta, 1+\delta, -(1-\delta)].$$

Figure 11 shows our calculated band structures of the bcc lattice (thin red curves) and the bct lattice (thick blue curves). There is a clear difference between the two sets of band structures. In particular, around the Γ point, we observe a clear band splitting due to the difference in the crystal potential between the bcc and bct structures. This splitting occurs near the Fermi level and is thus expected to affect the low-energy properties.

Figure 12 depicts the calculated electronic DOS, with the inset depicting the magnification of the low-energy regime. We observe an increase in the DOS at the Fermi level $N(0)$ from the bcc to the bct structures. Here, the value of $N(0)$ is 1.466 (states/eV/atom) for bcc and 1.540 (states/eV/atom) for bct. The order of the present bcc value is reasonably consistent with the past theoretical result.[48] For reference, we performed the same calculation assuming lattice deformation of from the bcc to the body-centered orthorhombic

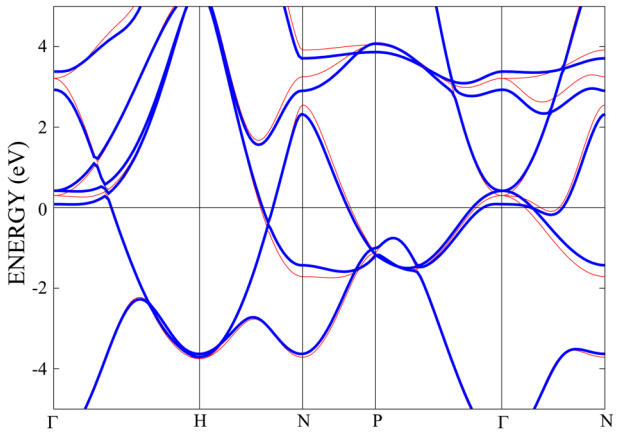

FIG. 11. Calculated band structures of the bcc lattice (thin red curves) and the bct lattice (thick blue curves). The Fermi level is zero.

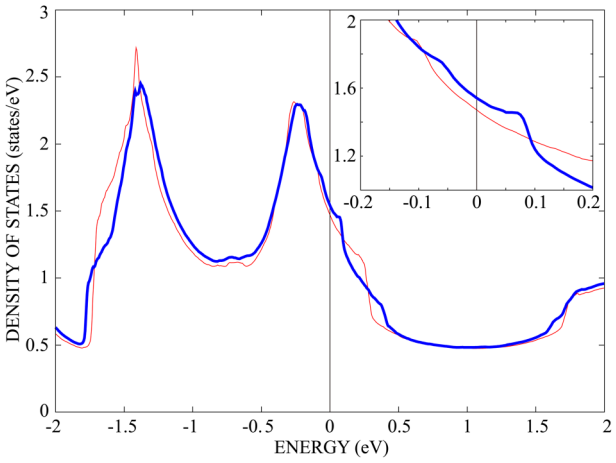

FIG. 12. Calculated electronic density of states of the bcc lattice (thin red curves) and the bct lattice (thick blue curves). The inset depicts the magnified portion around the Fermi level.

(bco) structures as $(a, a, a) \rightarrow (1.015a, 1.008a, 0.985a)$ so that we obtained the results similar to those for the bcc-bct deformation.

According to McMillan's theoretical work for strong-coupled superconductors, the electron-phonon coupling of the bcc 4d transition-metal superconductors is strengthened with the increase in $N(0)$.[49] An increase in the electron-phonon coupling constant as well as that in $N(0)$ contribute to the increase in T_c. Consequently, we speculate that the observed $N(0)$ increase due to deformation contributes to the experimental trend of T_c increase.

V. DISCUSSION

Our results have us reconfirm that $T_c(P)$ depends on both the initially accumulated strain and the HP quality (that is, the type of PTM used). Indeed, our data do not reproduce the representative results for Nb by Struzhkin *et al.*,[41] because the aforementioned two qualities are inequivalent between two experiments. In our study, eight kinds of samples were prepared, and for HPT($N = 10$)-Nb, three types of PTMs were used. Our experimental results present two important phenomena: (1) initial strengthening of intergrain coupling in weakly coupled Josephson array enhances T_c and (2) afterwards anisotropic lattice deformation can enhance T_c effectively. In the HPT($N = 10$)-Nb sample, $T_c(P \sim 2\,\text{GPa})$ exceeded 9.9 K. Below, we discuss the present experimental results from the viewpoints of both the intergrain network and the lattice distortion.

Pressure effects on intergrain superconducting network. Bulk phase coherence exists on the so-called Josephson array. When Josephson coupling is weakened, bulk T_c decreases. In the light HPT processing such as AR $\rightarrow$ HPT($N = 1$), the storage of dislocations brings about the decrease in grain size and weakens the superconducting junction between grains. The prominent effect in pressure application of a few GPa level to HPT($N = 1$) appears in the pressure region exhibiting isotropic lattice shrinkage, and it originates from strengthening intergrain coupling via grain boundaries. In $YBa_2Cu_4O_8$[2,3] and $YBa_2Cu_3O_7$[3] ceramics with a weakly coupled random Josephson network, T_c increases with strengthening the intergrain coupling. This effect is expected to be enhanced in a system with smaller grain size.[1] As N increases like $1 \rightarrow 2 \rightarrow 5 \rightarrow 10$, the intergrain network becomes strong along with the formation of the large-angle grain boundaries. There, the strength of intergrain coupling does not change largely under pressures. As seen in Table II, the largest shrinkage ratio at the unit-cell level is indeed observed in AR-Nb, which indeed has some residual strain. With release in the residual strain by melting and the application of a small amount of HPT [i.e. HPT($N = 1$)], the shrinkage ratio becomes small. Further, the HPT process turns to an increase in the shrinkage ratio. We might be able to suppose that in HPT($N = 1$), the compression force was actually used for intergrain compression as well as lattice shrinkage.

Pressure effects on lattice distortion. The characteristic difference in the HP response between HPT($N = 5$) and HPT($N = 10$) and that between HPT($N = 10$) using solid PTM and HPT($N = 10$) using liquid PTM cannot be understood with the above scenario considering the change in the intergrain network. According to band energy calculations, a reduction in the crystal symmetry from bcc to bct leads to an increase in the DOS near the Fermi energy, which forms a key factor contributing to an increase in T_c. The results of a previous XRD experiment by Takemura and Singh have already indicated that Nb intrinsically exhibits the characteristic of reduction in the structural symmetry at a characteristic pressure (P_c') under non-ideal HP conditions ($P_c' \sim 10$ GPa with the use of MEW).[41] Indeed, as per magnetic measurements obtained with the use of NaCl as the PTM by Struzhkin *et al.*, T_c exhibits a peak of 9.9 K around 10 GPa.[41] Interestingly, there is a consistency between two experiments. Against the backdrop of these reported results, our results indicate that the additional insertion of residual strain in the targeted samples induces a P_c' shift toward the lower-pressure side. For instance, the HPT-Nb ($N = 10$) sample in our study exhibited a T_c of 9.8-9.9 K at a pressure of a few GPa. Subsequently, as the HP quality deteriorated, P_c determined by the magnetic measurement decreased, and the T_c value at P_c increased. Here, we stress that non-ideal HP conditions are effective in optimizing T_c of Nb at low pressures. Indeed, in our study, we applied anisotropic stress to the samples in the solidified condition, wherein the stress applied to the sample was not isotropic. The peak T_c at P_c was observed in all of the measured samples. We posit here that the use of liquid helium as the PTM would lead to a large increase in P_c ($P_c \gg 10$ GPa): For the AR and HPT($N = 1$, 5, and 10) samples, in which a large amount of strain was accumulated, a large reduction in the crystal symmetry was indeed observed near P_c in the XRD experiments. However, the present XRD data of the ARC, HPT($N = 1$), and HPT($N = 10$) samples with the use of MEW as the PTM indicate that it is difficult to explain the pressure dependence of T_c using only the structural data at the unit-cell level. Indeed, there is a limitation to the experimental accuracy in determining the structural parameters. We speculate that the strain at the grain-size level would also need to be considered for detailed discussions. Meanwhile, a primary study finding is the availability of a new approach to increase T_c via the anisotropic structure change.

Finally, we discuss the two important aspects of sample quality: purity and residual strain. In the field of condensed matter physics, the sample purity is desired to be highly important, while

the residual strain in the sample plays a key role in material engineering as discussed from the viewpoint of microstructure. The latter effect appears at both the intergrain network and the unit-cell level. The difference in T_c at $P = 0$ across samples is possibly related to microstructure properties such as the average grain size and intergrain network.[8] Our experimental results indicate that the HP response of the T_c should be elucidated from both perspective of the intergrain network and that of the distortion of the unit cell. In particular, the trend of an increase in T_c due to the anisotropic structure change is understood by the observed increase in DOS at the Fermi energy.

VI. CONCLUSION

We investigated the pressure dependence of the T_c of Nb samples by varying both the effective sample quality and the HP quality, and we found that Nb generally tended to exhibit a structural deformation from the bcc to a strained bcc like tetragonal system with a lower structural symmetry. In non-severely strained Nb, the strengthening of intergrain coupling enhances T_c. In severely strained Nb, the above lattice deformation brings about an increase in T_c. The latter approach offers an artificial route to increase T_c. A large amount of strain and poor HP quality can cause this structural deformation to occur at low pressures. The reduction in the structural symmetry from cubic to tetragonal-like leads to an increase in the DOS at the Fermi energy. In the case of Nb, the maximum T_c is 9.92 K for samples subjected to the HPT procedure, where the revolution number is 10 and the stress is applied under solidified conditions. Thus, from the viewpoint of material engineering as well as pure physics, we were able to manipulate the T_c variations.

ACKNOWLEDGMENTS

This work was supported by MEXT KAKENHI, a Grant-in-Aid for Scientific Research on Innovative Areas "Bulk Nanostructured Metals" (No. 25102709) and a Grant-in-Aid for Scientific Research (S) (No. 26220909). This work was also supported by JSPS KAKENHI (Grant Nos. 16H04338, 16K05460, and 17H03379). The HPT process was carried out at the International Research Center on Giant Straining for Advanced Materials (IRC-GSAM) in Kyushu University.

REFERENCES

[1]J. Mayoh and A. M. García-García, Phys. Rev. B **90**, 134513 (2014).
[2]H. Deguchi, K. Koyama, M. Yasunaka, S. Takagi, N. Nagano, and K. Mizuno, J. Phys. Chem. Solid **63**, 1081 (2002).
[3]K. Koyama, H. Deguchi, S. Takagi, and K. Mizuno, J. Low Temp. Phys. **131**, 595 (2003).
[4]J. S. Schilling, in *Handbook of High-Temperature Superconductivity*, edited by J. R. Schrieffer (Springer, New York, 2007), pp. 427–462.
[5]I. Bashkin, V. Tissen, M. Nefedova, and E. Ponyatovsky, Physica C **453**, 12 (2007).
[6]M. Strongin, Physica **55**, 155 (1971).
[7]J. K. Hulm and B. B. Goodman, Phys. Rev. **106**, 659 (1957).
[8]T. Nishizaki, S. Lee, Z. Horita, T. Sasaki, and N. Kobayashi, Physica C **493**, 132 (2013).
[9]M. Mito, H. Matsui, K. Tsuruta, T. Yamaguchi, K. Nakamura, H. Deguchi, N. Shirakawa, H. Adachi, T. Yamasaki, H. Iwaoka *et al.*, Sci. Rep. **5**, 36337 (2016).
[10]R. Valiev, Y. Estrin, Z. Horita, T. Langdon, M. Zehetbauer, and Y. Zhu, JOM **58**, 33 (2006).
[11]R. Valiev, R. Islamgaliev, and I. Alexandrov, Prog. Mater. Sci. **45**, 103 (2000).
[12]P. W. Bridgman, Phys. Rev. **48**, 825 (1935).
[13]N. A. Smirnova, V. I. Levit, V. I. Pilyugin, R. I. Kuznetsov, L. S. Davydova, and V. A. Sazonova, Fiz. Metal. Metalloved. **61**, 1170 (1986).
[14]Y. Harai, Y. Ito, and Z. Horita, Scr. Mater. **58**, 469 (2008).
[15]K. Edalati and Z. Horita, Mater. Sci. Eng. A **652**, 325 (2016).
[16]V. M. Segal, V. I. Reznikov, A. E. Drobyshevskiy, and V. I. Kopylov, Russ. Metall. **1**, 99 (1981).
[17]A. Azushima, R. Kopp, A. Korhonen, D. Yang, F. Micari, G. Lahoti, P. Groche, J. Yanagimoto, N. Tsuji, A. Rosochowski *et al.*, CIRP Ann. Manuf. Tech. **57**, 716 (2008).
[18]Y. Saito, H. Utsunomiya, N. Tsuji, and T. Sakai, Acta Mater. **47**, 579 (1999).
[19]A. Zhilyaev and T. Langdon, Prog. Mater. Sci. **53**, 893 (2008).
[20]S. Bose, P. Raychaudhuri, R. Banerjee, P. Vasa, and P. Ayyub, Phys. Rev. Lett. **95**, 147003 (2005).
[21]W. E. Gardner and T. F. Smith, Phys. Rev. **144**, 233 (1966).
[22]W. Gey and G. van Heyden, Z. Phys. **193**, 65 (1966).
[23]D. Köhnlein, Z. Phys. **208**, 142 (1968).
[24]W. Gey, Z. Phys. **229**, 85 (1969).
[25]N. B. Brandt and E. Papp, Sov. Phys. J. Exp. Theor. Phys. **30**, 595 (1970), available at http://www.jetp.ac.ru/cgi-bin/dn/e_030_04_0595.pdf.
[26]T. F. Smith, Phys. Lett. **33**, 465 (1970).
[27]V. V. Struzhkin, Y. A. Timofeev, R. J. Hemley, and H. kwang Mao, Phys. Rev. Lett. **79**, 4262 (1997).
[28]S. Bose, P. Raychaudhuri, R. Banerjee, and P. Ayyub, Phys. Rev. B **74**, 224502 (2006).
[29]S. Lee and Z. Horita, Mater. Trans. **53**, 38 (2012).
[30]K. Edalati, J. M. Cubero-Sesin, A. Alhamidi, I. Mohamed, and Z. Horita, Mater. Sci. Eng. A **613**, 103 (2014).
[31]P. Das, C. V. Tomy, S. S. Banerjee, H. Takeya, S. Ramakrishnan, and A. K. Grover, Phys. Rev. B **78**, 214504 (2008).
[32]T. Tomita, J. S. Schilling, L. Chen, B. W. Veal, and H. Claus, Phys. Rev. B **74**, 064517 (2006).
[33]A. W. Webb, D. U. Gubser, and L. C. Towle, Rev. Sci. Instrum. **47**, 59 (1976).
[34]M. Ishizuka, M. Iketani, and S. Endo, Phys. Rev. B **61**, R3823 (2000).
[35]M. Mito, M. Hitaka, T. Kawae, K. Takeda, T. Kitai, and N. Toyoshima, Jpn. J. Appl. Phys. **40**, 6641 (2001).
[36]I. Fujishiro, G. J. Piermarini, S. Block, and R. G. Munro, in *High Pressure in Research and Industry: Proceedings of the 8th AIRAPT Conference*, edited by C. M. Backman, T. Johannisson, and L. Tegner (Arkitektkopia, Uppsala, Sweden, 1982), Vol. II, p. 608.
[37]G. J. Piermarini, S. Block, J. D. Barnett, and R. A. Forman, J. Appl. Phys. **46**, 2774 (1975).
[38]A. Fujiwara, K. Ishii, T. Watanuki, H. Suematsu, H. Nakao, K. Ohwada, Y. Fujii, Y. Murakami, T. Mori, H. Kawada *et al.*, J. Appl. Cryst. **33**, 1241 (2000).
[39]T. Varga, A. P. Wilkinson, and R. J. Angel, Rev. Sci. Instrum. **74**, 4564 (2003).
[40]Y. A. Freiman and H. J. Jodl, Phys. Rep. **401**, 1 (2004).
[41]K. Takemura and A. K. Singh, Phys. Rev. B **73**, 224119 (2006).
[42]J. Yamauchi, M. Tsukada, S. Watanabe, and O. Sugino, Phys. Rev. B **54**, 5586 (1996).
[43]N. Troullier and J. L. Martins, Phys. Rev. B **43**, 1993 (1991).
[44]L. Kleinman and D. M. Bylander, Phys. Rev. Lett. **48**, 1425 (1982).
[45]J. P. Perdew, K. Burke, and M. Ernzerhof, Phys. Rev. Lett. **77**, 3865 (1996).
[46]T. Fujiwara, S. Yamamoto, and Y. Ishii, J. Phys. Soc. Jpn. **72**, 777 (2003).
[47]Y. Nohara, S. Yamamoto, and T. Fujiwara, Phys. Rev. B **79**, 195110 (2009).
[48]K. H. Lee and K. J. Chang, Phys. Rev. B **54**, 1419 (1996).
[49]W. L. McMillan, Phys. Rev. **167**, 331 (1968).